Orientational Order and Alignment of Elongated Particles Induced by Shear

Tamás Börzsönyi,[1,*] Balázs Szabó,[1] Gábor Törös,[1] Sandra Wegner,[2] János Török,[3] Ellák Somfai,[4] Tomasz Bien,[2] and Ralf Stannarius[2]

[1]*Institute for Solid State Physics and Optics, Wigner Research Center for Physics, Hungarian Academy of Sciences, P.O. Box 49, H-1525 Budapest, Hungary*

[2]*Otto-von-Guericke-University, D-39106 Magdeburg, Germany*

[3]*Faculty of Physics, University of Duisburg-Essen, 47048 Duisburg, Germany*

[4]*Department of Physics and Centre for Complexity Science, University of Warwick, Coventry CV4 7AL, United Kingdom*

(Received 23 August 2011; published 30 May 2012)

Shear induced alignment of elongated particles is studied experimentally and numerically. We show that shear alignment of ensembles of macroscopic particles is comparable even on a quantitative level to simple molecular systems, despite the completely different types of particle interactions. We demonstrate that for dry elongated grains the preferred orientation forms a small angle with the streamlines, independent of shear rate across three decades. For a given particle shape, this angle decreases with increasing aspect ratio of the particles. The shear-induced alignment results in a considerable reduction of the effective friction of the granular material.

DOI: 10.1103/PhysRevLett.108.228302 PACS numbers: 47.57.Gc, 45.70.−n

Flow of large ensembles of elongated objects—often observed in nature or industry—usually induces pronounced alignment of the building blocks. This phenomenon is found at all length scales: in log jams on rivers, in slowly deformed multi-component clastic rocks, in seeds, nanorods, and viruses, and even at molecular scales in nematic liquid crystals [1–17]. On one hand, such alignment processes are poorly characterized for macroscopic objects, even though granular flows have been extensively studied in the last two decades [14–29]. On the other hand, shear alignment and collective reorientation dynamics is well documented and exploited at the molecular scale (for nematic liquid crystals) and can be described quantitatively by continuum theory [30,31]. Studies have also shown that the stationary alignment observed for simple one-component systems may be replaced by a so called *tumbling* behavior for more complex materials, e.g., nematic liquid crystals with pretransitional smectic fluctuations [10,31–33], polymeric liquid crystals [34–37], and dilute suspensions where individual particles rotate in shear flows (Jeffery orbits, [38]). For the limiting case of very dense suspensions, direct interparticle forces dominate leading to stationary flow alignment, which is analogous to what is expected for simple one-component systems.

In this study we focus on simple one-component systems and aim to bridge the gap between systems of very different sizes and interaction types. Our goal is to determine the shear induced order and average orientational angle for macroscopic objects, to track how the phenomenon depends on the particle aspect ratio, and find to what extent the applied shear rate is relevant. Starting from an initially random orientation, we also aim to quantify the change in the shear resistance of a sample because of the evolving alignment.

We sheared the granular material in a cylindrical split bottom geometry (see Fig. 1) where stationary flow is obtained by a continuous rotation of a thin plate below the material. The strain is localized [26,27,39] in the so called "shear zone" (indicated with dark gray). In this geometry the time and ensemble averaged shear rate changes with the radius in a relatively wide region

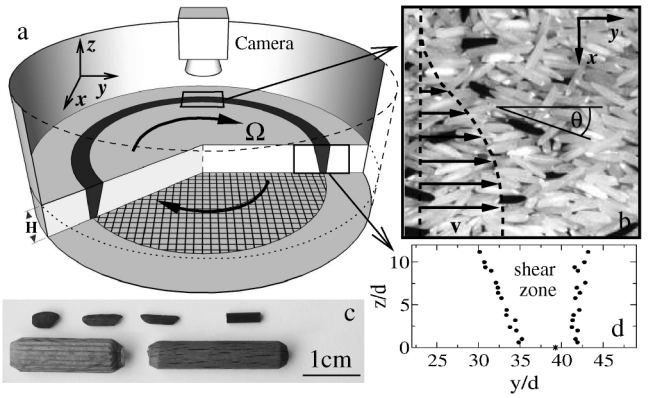

FIG. 1. (a) Schematic illustration of the split bottom shear cell [26]. The granular material consisting of elongated grains with mean diameter d and length L is sheared because of the rotation of the thin circular plate below the material with diameter $D_p \approx 80d$ and angular velocity Ω. The container diameter is $D_c \approx 140d$, while typical filling height is $H \approx 11d \approx 0.14D_p$ (unless stated otherwise). Shear deformation is localized at the region marked with dark gray. (b) Particles are oriented on average at a small angle θ with respect to the streamlines. (c) Photographs of the particles studied, with $L/d = 2.0$, 3.4, 4.5 (rice), as well as 3.5 (glass cylinders), and 3.3, 5.0 (pegs). (d) Measured borders of the shear zone for pegs with $L/d = 5.0$ (border defined at approximately 10% of the maximum shear rate).

allowing us to map the shear rate dependence of the alignment in a single experiment [28]. Prolate particles with different length to diameter ratios L/d were investigated [Fig. 1(c)]. Two methods were used to visualize and evaluate shear-induced alignment: (i) complete 3D imaging of the sample with x-ray tomography, and (ii) optical imaging of the particles at the upper surface of the system with a digital camera. For the characterization of changes in effective friction because of the alignment, the torque on the bottom plate was measured at stationary rotation. The experiments were complemented with numerical simulations using the discrete element method (DEM). In the simulations elongated particles were prepared by numerous overlapping spheres and the alignment of the particles was measured in plane Couette flow.

The shear-induced orientational order is monitored by diagonalizing the symmetric traceless order tensor $\boldsymbol{T}$

$$T_{ij} = \frac{3}{2N}\sum_{n=1}^{N}\left[\ell_i^{(n)}\ell_j^{(n)} - \frac{1}{3}\delta_{ij}\right], \qquad (1)$$

where $\vec{\ell}^{(n)}$ is a unit vector along the long axis of particle n, and the sum is over all N detected particles. The largest eigenvalue of $\boldsymbol{T}$ is taken as the primary order parameter S. A second, biaxial order parameter D is defined as the difference of the two other eigenvalues of $\boldsymbol{T}$. The shear-induced alignment is characterized by the average alignment angle θ_{av} measured with respect to the shear flow direction [see Fig. 1(b)], i.e., the deviation of the largest main axis of $\boldsymbol{T}$ from the streamlines.

First, we present the shear rate dependence of the average alignment angle θ_{av} and the order parameter S obtained by digital optical imaging at the surface layer. In this experiment, the shear zone at the top was divided into 15 bands (with widths of 0.19 cm $\approx d$) and the average shear rate was determined for each band. The orientation and in-plane length of colored tracer particles (6% of the sample) were detected with a particle tracking code, yielding about 60,000 particle positions in each band. The center θ_{av} of the orientational distribution was determined by fitting a Gaussian, and the order parameter S was calculated. These two quantities are shown for the roughly ellipsoidal rice grains in Figs. 2(a) and 2(b) as a function of the shear rate $\dot{\gamma}$. Here the shear rate spans a wide range of inertial numbers—about 0.0002 to 0.4—using three different rotation rates of the bottom plate ($\Omega = 0.26$, 0.52 and 4.2 rad/s) and considering the spatial variation of $\dot{\gamma}$ in the shear zone. The ranges of $\dot{\gamma}$ spanned for each Ω are indicated with horizontal bars in Fig. 2(a). (The inertial number [21] is defined as $I = \dot{\gamma}d\sqrt{\rho/P}$, where ρ is the density of particles and P is the pressure.)

As it is seen, θ_{av} is well defined, and it is essentially independent of the shear rate for the whole range of $\dot{\gamma}$ investigated here. This result is not unexpected; it is actually similar to the case of flow aligning nematic liquid crystals consisting of elongated molecules, where the

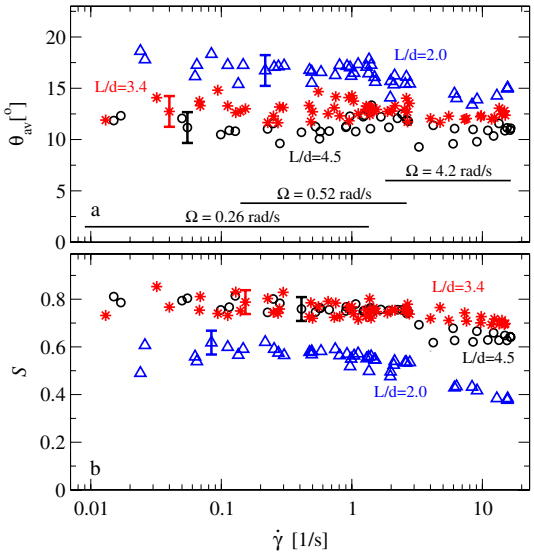

FIG. 2 (color online). (a) The average orientational angle θ_{av} of the particles with respect to the streamlines and (b) the order parameter S as a function of the shear rate $\dot{\gamma}$. Both panels correspond to optical measurements for rice grains with length to width ratios $L/d = 2.0$, 3.4, and 4.5. The value of θ_{av} is roughly constant, and S varies only very weakly across three decades of the shear rate.

alignment angle is a material parameter, i.e., shear rate independent as well. But even if the aspect ratios of the building blocks (molecules and granulates) are similar, the interparticle forces have very different characteristics in these two systems. While the molecules experience attractive forces (dipole-dipole, van der Waals), the grains investigated here interact only via hard core repulsion and friction. The fact that despite these differences the alignment angle is independent of the shear rate underlines the robustness and the geometrical origin of the shear alignment. The slightly decreasing value of the order parameter S with increasing shear rate [Fig. 2(b)] shows that the inertial effects make the material less ordered while preserving the same alignment direction.

The numerical simulations were performed using DEM, where long particles were approximated by chains of overlapping spheres. Special care was taken to reduce the possible interlocking of neighboring chains: both the overlap (30%–70%) and the number of participating spheres were varied randomly. For implementing a soft particle model we used the general purpose molecular dynamics code LAMMPS [40], extended with particle cementing interactions within the chains [29] without allowing the contacts to break. An assembly of 600–1200 elongated particles was confined under constant pressure between two parallel, rough walls of finite mass; the system was periodic in the other two directions. The shear flow was realized by imposing a fixed and opposing velocity of the walls. In the steady state the shear velocity profiles were reasonably linear to neglect shear rate variations.

The inertial number was in the range from 0.004 to 0.09. To calculate the average alignment angle and order parameter, only the central 60% was considered in order to exclude influences of the walls.

The complete 3D arrangement of all particles in the shear zone was also determined experimentally for two samples (pegs with $L/d = 3.3$ and 5.0) using x-ray tomography [41]. The purpose of these experiments is to show that the order and alignment data extracted from surface particles are representative for the global order in the shear zone, with only slight variations. The particles were detected by applying a watershed algorithm to the recorded images. The components of $\boldsymbol{T}$ were determined for a surface region of $\sim$1 cm (two particle diameters) depth and for a 2 cm thick layer below (bulk), corresponding to about 10000 and 20000 particle positions, respectively.

Figure 3 combines the bulk and surface results from x-ray tomography, the surface data from optical experiments, and the numerical results. Comparing the average values of the shear alignment angle for the six samples investigated, we find a systematic decrease of θ_{av} with increasing length to width ratio [Fig. 3(a)] for a given material (rice or cylinders). At comparable aspect ratios, the alignment angle appears to be smaller for cylinders (as if they had a larger effective aspect ratio). Figure 3(b) shows that the alignment angle θ_{av} displays a decreasing

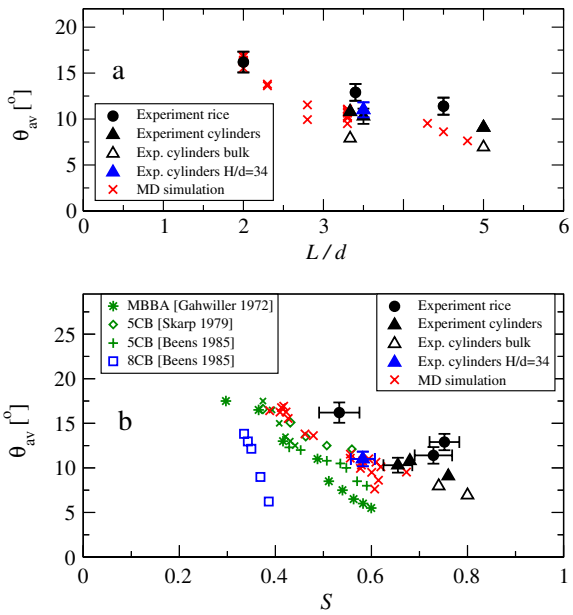

FIG. 3 (color online). The average orientational angle θ_{av} as a function of the (a) length to diameter ratio L/d of the particles and (b) order parameter of the system obtained by experiments (●, ▲, △) and numerical simulations (×). One datum point (blue ▲) was taken with a particularly deep layer, $H/d = 34$. The alignment angles for typical flow aligning nematic liquid crystals MBBA and 5CB (*, ◇, +) [8–11,46] and for a nematic liquid crystal 8CB (□) which shows tumbling when approaching the smectic-A phase transition are shown for comparison.

trend with increasing order parameter for both experiment and simulation. The measurement with $H/d = 34$ shows that the value of θ_{av} is independent of H. The orientational order slightly increases with decreasing H, which may be an interesting subject for further investigations. As a possible explanation for the trends observed in Figs. 3(a) and 3(b), we suggest the following picture: in a dense granular system, the elongated particles are entangled with neighbors that hinder their rotation. In a shear flow an orientation distribution develops because of the competition between the agitations by collisions and this hindering effect. The orientation angles of the particles have a distribution centered around θ_{av}, where the width of the distribution roughly equals θ_{av}. For more elongated and therefore more entangled particles the angular fluctuations will be smaller, so the width of the distribution is smaller, making θ_{av} smaller.

The x-ray tomograph measurements confirm that the shear alignments at the surface and in the bulk are very similar, with slightly larger order parameter S and slightly smaller alignment angle θ_{av} in the bulk [see Figs. 3(a) and 3(b)]. The slightly larger order observed in the bulk is connected to a smaller standard deviation from the mean orientation within the shear plane (while the out-of-plane standard deviation is similar in the bulk and at the surface). This is in good agreement with molecular dynamics simulations of a hard spheroid fluid under shear flow [42], where a similar biaxiality was detected. For our case the measured biaxiality is somewhat stronger in the bulk ($D \approx 0.09$) than at the surface ($D \approx 0.03$).

For comparison, we have also included the order parameter dependence of the alignment angle for typical flow aligning nematic liquid crystals (MBBA and 5CB) for which the aspect ratio of the molecular shape is estimated to be $L/d = 2.5$ [11]. For molecular nematics the order parameter is independent of the shear rate (in this case determined by the temperature). We emphasize that the decreasing tendency of the $\theta_{\mathrm{av}}(S)$ curves is very similar for granulates and for these nematics. We also note that different flow behavior is observed for some nematics that exhibit strong smectic fluctuations when approaching the smectic-A phase transition [10,31–33]. For example, nematic 8CB shear aligns only in a narrow temperature range near the clearing point. With decreasing temperature, the θ_{av} curve approaches zero when one of the viscosity coefficients changes sign, 5.6 K above the transition to smectic-A (where $S \approx 0.4$). Pretransitional smectic clusters drive the system into a tumbling behavior, where the director continuously rotates in the shear flow. Another example for tumbling is the case of polymeric liquid crystals, where the presence of polymeric chains strongly modifies the flow behavior [34–37]. For molecular systems the flow behavior of the aligned case as well as the dynamical modes of the tumbling state can be accurately characterized by modern experimental tools, such as x-ray scattering [34–36], NMR [34,37] or conoscopy [32],

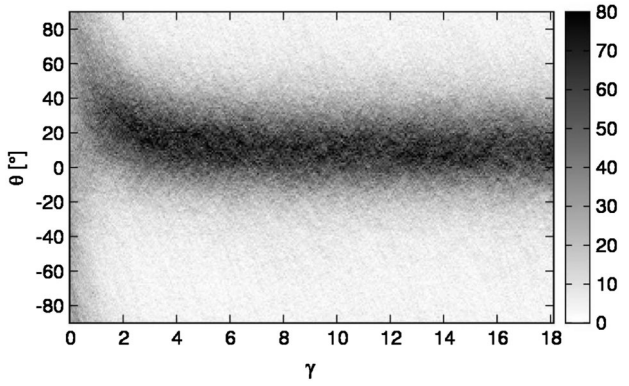

FIG. 4. Evolution of the orientational distribution of the particles starting from an initially random orientation.

and non-equilibrium molecular dynamics simulations [33,42]. Various theories have also predicted the instabilities and different dynamical modes, like tumbling, kayaking, wagging, log rolling, or flow aligning [43–45]. These theories are more general in the sense that they map the phase diagram not only as a function of aspect ratio, but also as a function of density including the case of dilute systems as well. They predict flow alignment for our parameter range [43,44]. Altogether, the fact that stationary alignment is observed in our dense granular system—with no detectable smectic fluctuations and simple interactions between the particles—is in agreement with the above observations and theories.

The initial evolution of order has been measured starting from a randomly oriented configuration. Data were obtained from 1300 experiments. The orientational distribution is presented in Fig. 4 as a function of the strain taken in the middle part of the shear zone for a sample with $L/d = 3.5$. As it is seen, order develops quickly and the alignment angle θ_{av} decreases towards the stationary value. The strong decrease of θ_{av} at the beginning of the process is a consequence of the fact that the vast majority of particles rotate in the same direction because of the shear flow. The transient in Fig. 4 evidences that an equilibrium alignment is established after the sheared particles have passed approximately three to four neighbors.

The increasing orientational order and the development of the shear alignment angle leads to a systematic change of the effective friction of the sample at the beginning of the process. This can be quantified by measuring the torque M needed to rotate the circular bottom plate with a constant speed. As a reference we have also recorded the torque for nearly spherical mustard seeds. This helps us to correct for the transient effects which are not directly related with orientational changes. The signals were corrected by subtracting the torque needed for rotating the empty plate, and rescaled by the stationary value M_∞. The rescaled torque $\tilde{M} = M/M_\infty$ is shown in Fig. 5(a), while Fig. 5(b) presents the curves for the elongated grains after subtraction of the data for mustard seeds on a log-lin scale. The evolution

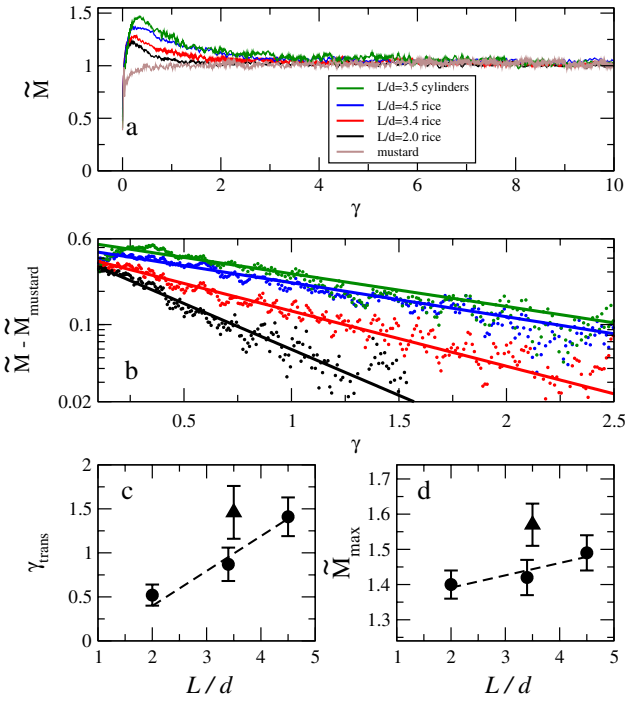

FIG. 5 (color online). (a)–(b) Evolution of the applied torque needed to maintain stationary rotation of the bottom plate starting from an initially random orientation. Panel (a) also includes a reference dataset obtained for spherical particles which is then subtracted from the other datasets resulting in the curves presented in panel (b). (c) Characteristic strain γ_{trans} corresponding to the transient and (d) ratio of the torques $M_{\mathrm{max}}/M_\infty = \tilde{M}_{\mathrm{max}}$ needed to rotate an unoriented sample and the oriented sample (stationary state) for rice (●), and cylinders (▲).

of the internal friction of the material can be characterized by an exponential decay of the excess torque as $\tilde{M} - \tilde{M}_{\mathrm{mustard}} \approx (\tilde{M}_{\mathrm{max}} - 1)e^{-\gamma/\gamma_{\mathrm{trans}}}$. The solid lines in Fig. 5(b) are exponential fits; they define a characteristic deformation γ_{trans} describing the transient. The dependence of γ_{trans} on the aspect ratio is shown in Fig. 5(c). For rice grains, the transients increase with grain length. This evidences a slower dynamics of the more elongated particles. A linear fit yields $\gamma_{\mathrm{trans}} = 0.4(L/d - 1)$ for rice. The ratio of the torques corresponding to the totally random and the oriented systems is estimated around $\tilde{M}_{\mathrm{max}} \approx 1.5$ as seen in Fig. 5(d).

In conclusion, we used surface optical imaging, bulk x-ray tomography, as well as numerical simulations to study the shear flow of elongated dry granular particles. We found that the particles quickly orient themselves around a preferred direction, which is at an angle from the streamlines. This angle is almost independent of the shear rate (or inertial number) across three decades, and for a given class of shapes (rice or cylinders) it decreases with increasing particle aspect ratio. This shear alignment is a robust phenomenon, and its geometric origin is underlined by the similarity with nematic liquid crystals, despite the

completely different interparticle forces. The shear alignment decreases the effective friction by about one third when compared to the initial randomly oriented state.

The authors are thankful for G. Rose, chair of the department for Healthcare Telematics and Medical Engineering of the Otto von Guericke University, Magdeburg, and appreciate discussions with H. Brand, K. Daniels, A. Jákli, A. Krekhov, and H. Pleiner. J. T. acknowledges the support of the German Research Foundation (DFG Grant No. BR 3729/1). T. B. acknowledges Magdeburg University for a visiting grant.

*borzsonyi.tamas@wigner.mta.hu

[1] A. W. K. Ma, F. Chinesta, and M. R. Mackley, J. Rheol. **53**, 547 (2009).
[2] W. J. Orts, in *Flow-Induced Structure in Polymers*, edited by A. I. Nakatani and M. D. Dadmun (Oxford Univ. Press, New York, 1995), p. 335.
[3] D. M. Kuncicky, R. R. Naik, and O. D. Velev, Small **2**, 1462 (2006).
[4] A. Fahmi, H. Brünig, R. Weidisch, and M. Stamm, Macromol. Mater. Eng. **290**, 136 (2005).
[5] T. A. Lenstra, Z. Dogic, and J. K. G. Dhont, J. Chem. Phys. **114**, 10151 (2001).
[6] M. P. Lettinga, Z. Dogic, H. Wang, and J. Vermant, Langmuir **21**, 8048 (2005).
[7] E. Brown, H. Zhang, N. A. Forman, B. W. Maynor, D. E. Betts, J. M. DeSimone, and H. M. Jaeger, Phys. Rev. E **84**, 031408 (2011).
[8] K. Skarp, S. T. Lagerwall, B. Stebler, and D. McQueen, Phys. Scr. **19**, 339 (1979).
[9] C. Gähwiller, Phys. Rev. Lett. **28**, 1554 (1972).
[10] W. W. Beens and W. H. de Jeu, J. Chem. Phys. **82**, 3841 (1985).
[11] H. Ehrentraut and S. Hess, Phys. Rev. E **51**, 2203 (1995).
[12] N. W. Hayman, B. A. Housen, T. T. Cladouhos, and K. Livi, J. Geophys. Res. **109**, B05409 (2004).
[13] D. Karátson, O. Sztanó, and T. Telbisz, J. Sediment. Res. **72**, 823 (2002).
[14] R. P. Behringer and G. W. Baxter, in *Granular Matter, An Interdisciplinary Approach*, edited by A. Mehta (Springer, New York, 1994), p. 85.
[15] H. Ehrentraut and A. Chrzanowska, in *Dynamic Response of Granular and Porous Materials under Large and Catastrophic Deformations*, edited by K. Hutter and N. P. Kirchner (Springer, Berlin, 2003), p. 343.
[16] A. A. Peña, R. García-Rojo, and H. J. Hermann, Granular Matter **9**, 279 (2007).
[17] C. S. Campbell, Phys. Fluids **23**, 013306 (2011).
[18] H. M. Jaeger, S. R. Nagel, and R. P. Behringer, Rev. Mod. Phys. **68**, 1259 (1996).
[19] I. S. Aranson and L. S. Tsimring, Rev. Mod. Phys. **78**, 641 (2006).
[20] P. Jop, Y. Forterre, and O. Pouliquen, Nature (London) **441**, 727 (2006).
[21] GDR MiDi Collaboration, Eur. Phys. J. E **14**, 341 (2004).
[22] W. Losert, L. Bocquet, T. C. Lubensky, and J. P. Gollub, Phys. Rev. Lett. **85**, 1428 (2000).
[23] F. da Cruz, S. Emam, M. Prochnow, J-N. Roux, and F. Chevoir, Phys. Rev. E **72**, 021309 (2005).
[24] T. Börzsönyi, R. E. Ecke, and J. N. McElwaine, Phys. Rev. Lett. **103**, 178302 (2009).
[25] E. Azéma and F. Radjaï, Phys. Rev. E **81**, 051304 (2010).
[26] D. Fenistein and M. van Hecke, Nature (London) **425**, 256 (2003).
[27] D. Fenistein, J. W. van de Meent, and M. van Hecke, Phys. Rev. Lett. **92**, 094301 (2004).
[28] S. Luding, Particuology **6**, 501 (2008).
[29] L. Brendel, J. Török, R. Kirsch, and U. Bröckel, Granular Matter (to be publised).
[30] F. M. Leslie, Adv. Liq. Cryst. **4**, 1 (1979).
[31] J. T. Jenkins, Annu. Rev. Fluid Mech. **10**, 197 (1978).
[32] P. T. Mather, D. S. Pearson, and W. R. Burghardt, J. Rheol. **39**, 627 (1995).
[33] S. Sarman and A. Laaksonen, J. Chem. Phys. **131**, 144904 (2009).
[34] H. Siebert, I. Quijada-Garrido, J. Vermant, L. Noirez, W. R. Burghardt, and C. Schmidt, Macromol. Chem. Phys. **208**, 2161 (2007).
[35] W. R. Burghardt, E. F. Brown, M. Lujan Auad, and J. A. Kornfield, Rheol. Acta **44**, 446 (2005).
[36] F. E. Caputo and W. R. Burghardt, Macromolecules **34**, 6684 (2001).
[37] S. M. Fan, G. R. Luckhurst, and S. J. Picken, J. Chem. Phys. **101**, 3255 (1994).
[38] G. B. Jeffery, Proc. R. Soc. A **102**, 161 (1922).
[39] J. A. Dijksman, E. Wandersman, S. Slotterback, C. R. Berardi, W. D. Updegraff, M. van Hecke, and W. Losert, Phys. Rev. E **82**, 060301 (2010).
[40] S. Plimpton, J. Comput. Phys. **117**, 1 (1995).
[41] The measurements were carried out with a medical angiography system, i.e., rotatioanal *c*-arm based x-ray device equipped with a flat-panel detector at the INKA-Lab of the Otto von Guericke University, Magdeburg (http://www.inka-md.de), with resolutions between 1.5 pixel/mm and 2 pixel/mm.
[42] X.-F. Yuan and M. P. Allen, Physica (Amsterdam) **240A**, 145 (1997).
[43] N. Kuzuu and M. Doi, J. Phys. Soc. Jpn. **53**, 1031 (1984).
[44] R. G. Larson, Macromolecules **23**, 3983 (1990).
[45] M. G. Forest and Q. Wang, Rheol. Acta **42**, 20 (2003).
[46] I. Chirtoc, M. Chirtoc, C. Glorieux, and J. Thoen, Liq. Cryst. **31**, 229 (2004).